Nonlinear Flow Behavior of Entangled Polymer Solutions: Yieldlike Entanglement−Disentanglement Transition

Prashant Tapadia and Shi-Qing Wang*

Maurice Morton Institute of Polymer Science and Department of Polymer Science, University of Akron, Akron, Ohio 44325

Received May 10, 2004; Revised Manuscript Received September 8, 2004

ABSTRACT: We have carried out controlled-stress experiments in addition to the conventional controlled-rate measurements to probe the nature of nonlinear flow behavior of entangled 1,4-polybutadiene solutions. The flow responses are found to be drastically different depending on whether the shear flow is imposed by applying a constant torque or a constant velocity on one of the two surfaces in a cone−plate flow cell. When the applied shear stress is of a comparable magnitude to the elastic plateau modulus of the entangled solutions, a sharp yieldlike constitutive transition is observed, revealing a discontinuous relationship between the shear rate and the shear stress. Following such an entanglement−disentanglement transition (EDT), the chain orientation appears to further increase as a function of time as evidenced by the rising normal stress N_1, reflecting a plausible coil−uncoil transition (C−UCT). The relaxation of N_1 consists of an initial rapid decay, likely due to chain recoil from the C−UCT and a subsequent slow decrease characteristic of its relaxation in the presence of chain entanglement below the EDT. The controlled-rate measurements reveal familiar stress plateau behavior in a range of over 3 decades in the apparent shear rate, much of which is inaccessible by the controlled-stress experiment in steady state.

I. Introduction

Nonlinear flow phenomena including the familiar shear thinning behavior of entangled polymers have been investigated extensively over the past 4 decades,[1−3] both experimentally[4−11] and theoretically.[12−19] The objective has been twofold: (a) to depict the structure of polymeric fluids in terms of the states of chain entanglement and conformation as a function of the flow condition and (b) to determine the relationship between the flow field and the corresponding stress fields in both transient and steady states. Since the establishment of the original Doi−Edwards tube model, several new concepts have been introduced to extend de Gennes' idea[20] of chain reptation for polymer flow. These efforts have produced a detailed theoretical description of rheological behavior of entangled polymers.

Because experiment has always found a monotonic flow curve between shear stress and shear rate,[9−11,15] theoretical works[14−18] have focused on improving the tube model to bring the theoretical prediction into agreement with the experimental observations. The current consensus appears to be that the constitutive relationship between shear stress and shear rate is continuous and monotonic for entangled polymers. The most recent version[18] of the refined Doi−Edwards tube theory endorses this view. The authors of ref 18 have also made a rather complete review of recent research activities; consequently, we omit detailed discussion of the previous theoretical studies.

It is worthwhile to briefly review the experimental situation. Consider shearing a molecularly homogeneous polymeric fluid between two parallel plates that are separated by a gap distance H as shown in Figure 1a. To provide an experimental test of any constitutive relationship, one usually imposes a velocity V on the upper plate, in expectation that a uniform shear rate equal to V/H would be generated across the sample thickness, and measures the shear stress through a force transducer. In steady state, imposing a constant plate velocity indeed would create a simple shear flow with a spatially uniform shear rate, provided that there is a one-to-one relationship between the shear stress and shear rate for the polymer sample under study. However, this controlled-strain or controlled-rate mode[21] of imposing a plate velocity to produce an apparent or

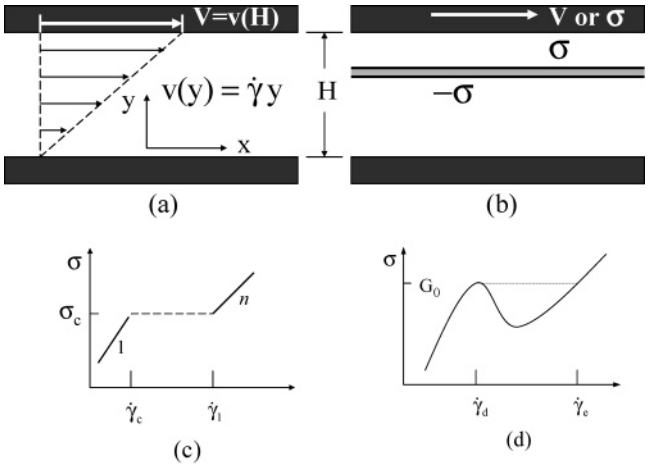

Figure 1. Schematic depictions of simple shear in idealized (i.e., in infinite $x-z$ dimensions) linearly displaced parallel plates where (a) a simple shear flow field with a uniform shear rate $\dot{\gamma}$ prevails; (b) the shear stress σ is indicated to be the same across the thickness, i.e., independent of y in steady state; (c) a sketch of a two-branch (with slopes of 1 and n) discontinuous constitutive curve characteristic of yieldlike behavior observable in the mode of imposed shear stress for sufficiently entangled monodisperse polymer solutions, where the dashed horizontal line is drawn in such a way as to indicate explicitly that there is no double-valuedness connecting the two branches; and (d) a schematic of a nonmonotonic constitutive curve according to ref 13.

* Corresponding author. E-mail: swang@uakron.edu.

10.1021/ma0490855 CCC: $27.50
Published on Web 10/27/2004

averaged shear rate is not suitable to delineate any constitutive yieldlike behavior,[22] where the shear rate $\dot{\gamma}$ rises abruptly at a critical stress σ_c as depicted in Figure 1c. When an apparent shear rate $\dot{\gamma}_a = V/H$ is imposed between $\dot{\gamma}_c$ and $\dot{\gamma}_1$, a sample possessing the same constitutive behavior as depicted in Figure 1c might be in a state of "frustration" or "metastability" because the sample cannot be uniformly sheared in steady state across the gap. Consequently, the protocol based on imposing constant velocity is potentially an unreliable method for exploring constitutive flow behavior of, and testing any theoretical constitutive predictions for, fluids for which it is unknown a priori whether the shear rate would jump discontinuously beyond a critical stress as depicted in Figure 1c.

A different protocol is crucial since we do not know whether well-entangled polymers undergo a yieldlike constitutive transition beyond a critical shear stress, where the sample might transform from a fully entangled state to a state of disentanglement. If such a transition would take place, measurements in the mode of imposing constant velocity would not reveal any signature of a flow transition and would actually produce a stress plateau, as seen previously in experiments.[9−11,15]

To examine this possibility and to avoid making any assumption about the qualitative features of the constitutive relationship governing entangled polymers, we first recognize that in steady state the shear stress is bound to be the same for any value of y because there is no acceleration in steady state in any layer such as that depicted in Figure 1b. Therefore, every value of shear stress is accessible and imposable, and every corresponding state of flow and state of fluid structure can be produced uniformly across the gap in steady state for homogeneous fluids. In a mode of imposing shear stress, the resulting shear rate is a freely adjusting variable. In other words, *imposing constant shear stress σ on the top plate can generate a uniform shear rate $\dot{\gamma}$ across the gap in steady state, provided that the steady state exists and the sample remains homogeneous under isothermal simple shear*. The preceding statement can be regarded as a theorem for isothermal simple shear of structurally homogeneous fluids in absence of any unstable or secondary flow. The condition that the sample is physically uniform and spatially homogeneous ensures that for every value of applied σ there is only one corresponding value of $\dot{\gamma}$ in steady-state simple shear. Our present experimental approach to entangled polymers including solutions is guided by this principle and is reliable provided that there is no shear-induced macroscopic inhomogeneity.

In passing, we note that the description of a discontinuous constitutive relationship given in Figure 1c is not necessarily the same as having a nonmonotonic constitutive curve as shown in Figure 1d. Consider the predictions of a nonuniform shear field in such a parallel plate flow cell according to the two different constitutive curves of Figure 1c,d. When imposing a velocity V such that $\dot{\gamma}_d H < V < \dot{\gamma}_e H$, the scenario of nonmonotonicity anticipated[12,13] coexistence of two bands where the sample would be sheared at $\dot{\gamma}_d$ and $\dot{\gamma}_e$, whereas the discontinuous constitutive curve depicted in Figure 1c may allow all shear rates between $\dot{\gamma}_d$ and $\dot{\gamma}_e$ to coexist across the sample thickness.

This paper focuses on making the first controlled-stress measurements in and beyond the Newtonian flow regime for entangled polymer solutions. As a reference, experiments with imposed constant velocity have also been performed to provide an illuminating comparison between the observed flow responses.

II. Experimental Section

A. Materials. For drag flow cells such as cone−plate and parallel plates, meniscus instability and distortion[23] are usually thought to be be avoidable only if the samples are sheared at sufficiently low stresses and shear rates. More importantly, commercially available rheometers are also limited to a low range of measurable shear and normal stresses. Thus, our entangled samples are solutions.

Previous studies[24,25] indicate that the elastic plateau modulus $G_{pl}(\phi)$ of an entangled solution can be lowered from that of the pure melt, G_N^0, according to $G_{pl}(\phi) = \phi^{2.2} G_N^0$. We can choose a sufficiently low volume fraction to substantially reduce the sample elasticity while still keeping a high level of chain entanglement. The degree of chain entanglement is measured in terms of the elastic plateau width, which is defined by the ratio of the terminal relaxation time τ_d to the tube constraint time τ_e, which is the cube of the number of entanglements per chain in the solution, given by $N/N_e(\phi)$. For solutions, this width is narrower than that of the pure melt according to[25] $\tau_d/\tau_e = [N/N_e(\phi)]^3 = (N/N_e)^3\phi^{3.6}$, where the cube of the number of entanglement per chain in the melt, $(N/N_e)^3$, is the plateau width of the pure melt.

For a model system that has enough entanglement, and yet is only weakly elastic, we have to select a polymer with an extremely high level of chain entanglement. This choice is a linear 1,4-polybutadiene (PBD) of $M_w = 1.24 \times 10^6$ g/mol and $M_w/M_n = 1.2$ from Polymer Source, Inc. We dissolve this linear PBD in the two slightly different solvents of phenyl-terminated oligomeric butadienes of M_n = 1K (oBD1) and M_n = 1.5K (oBD2) (Aldrich 20041-7 and 20048-4, respectively).

In this paper all measurements were made on a 10 wt % solution where the solvent is either oBD1 or oBD2. Since the densities of oBD1, oBD2, and PBD are sufficiently close, the volume fraction of PBD can be taken as $\phi = 0.1$. The critical molecular weight for entanglement in such a 10% solution is $M_e(\phi) = M_e\phi^{-1.2}$, where M_e is taken to be 1600 g/mol for 1,4-PBD. Thus, there are about $M_w/M_e(\phi) = 47$ entanglements per chain. All samples were prepared by dissolving the PBD and oBD in toluene to achieve molecular mixing before removing over 99.5% of the toluene in a vacuum oven at room temperature. Experiments in the mode of imposing constant velocity as described in section III.A are based on the 10% solution made of oBD1, and all data in section III.B are based on the 10% solution made of oBD2.

B. Apparatuses. A dynamic mechanical spectrometer (Advanced Rheometrics Expansion System-ARES) was used to obtain master curves for storage and loss moduli G' and G'' from a sequence of oscillatory shear measurements in a temperature range from 60 to −40 °C. The spectrometer is equipped with a 200−2000 g cm dual range, force rebalance transducer. Parallel plates with 25 mm were used for all the oscillatory shear measurements with ARES. Cone−plate is used for continuous shear, where the cone angle is 5.4° and the diameter is either 25, 15, or 8 mm.

A stress-controlled Bohlin-CVOR rheometer was employed in various modes. Cone−plate of the same geometry as those for ARES described in the preceding paragraph were used for Bohlin. Other cone angles of 2.4° and 8° were also employed for Bohlin and found to yield the same results as those obtained with the 5.4° angle. Cone−plate and parallel plates of 25 and 8 mm diameters were used for start-up shear measurements using the ARES. Specifically, all data in section III.A were collected using parallel plates at 40 °C, and data in section III.B were obtained with the cone−plate of 5.4° angle at 30 °C.

It should be remarked that the axial stiffness of the Bohlin-CVOR is such that there is no detectable gap change by measurement of a micrometer with sensitivity of 2 μm and by direct video imaging through a tele-micro-lens as long as the

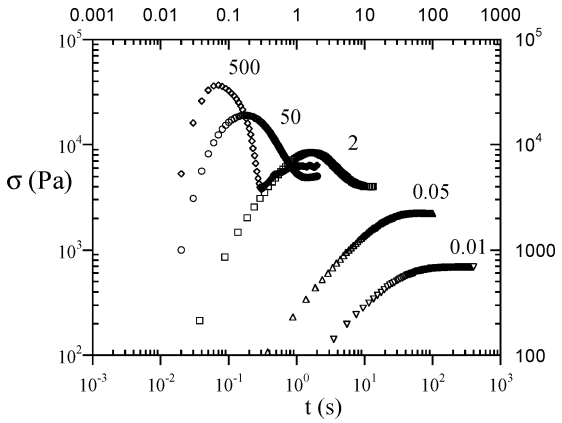

Figure 2. Stress growth in start-up shear experiments where various apparent shear rates were imposed in the Newtonian, plateau, and translational regimes, and the numbers near the curves indicate the apparent shear rate in the unit of s^{-1}.

normal force does not exceed 1.8 kg. This means that we could use a cone−plate of 15 mm diameter for shear stresses up 8.0 kPa, at which a normal stress of N_1 around 2×10^5 Pa is produced, as shown in Figure 6d in section III.

III. Primary Experimental Results and Discussion

A. Measurements in Mode of Imposing Constant Velocity. Stress Overshoot in Start-Up Shear. The flow behavior of entangled polymers is usually explored by imposing various constant velocities as depicted in Figure 1a and measuring the resulting stresses as a function of time. Using this traditional approach, the time-dependent stress growth is obtained for 10% PBD/oBD1 in Figure 2 upon start-up of shear in all three regions: Newtonian (i.e., terminal), plateau, and transitional. In the terminal region, the stress growth is monotonic as expected. Familiar stress overshoot is seen above the Newtonian region in agreement with previous observations.[9,11] Here only two shear rates of $\dot{\gamma}_a = 2$ and 50 s^{-1} are selected as examples of the stress overshoot that takes place in the so-called stress plateau region. Just beyond the stress plateau region, stress undershoot is observed to follow the overshoot. Other raw data similar to those in Figure 2 are omitted for clarity.

The steady-state stress values obtained in such start-up shear experiments are plotted in Figure 3 against the applied apparent shear rate $\dot{\gamma}_a$. It is striking to see the appearance of a stress plateau over 3 decades in Figure 3, which is similar to those[10] observed previously. It is instructive to also include all the data points corresponding to the maxima of the transient stress. The difference between the upper-filled and filled squares approximately depicts how the solution eventually avoids a shear stress buildup in the mode of imposing constant velocity. It is intriguing to notice that the steady-state shear stress remains saturated just below the elastic plateau modulus as indicated in Figure 3 by $|G^*|$ from oscillatory shear measurements.

Shear Quenching. Although the stress overshoot in the plateau region shown in Figure 3 has been reported previously for monodisperse entangled polymer solutions,[9,11] the nature of the shear flow in the plateau region has remained elusive. Here we perform shear-quench experiments to learn more about the phenomenology at the stress plateau. We first preshear the sample at various apparent rates in the plateau and transition regions and then "quench" to the lower end

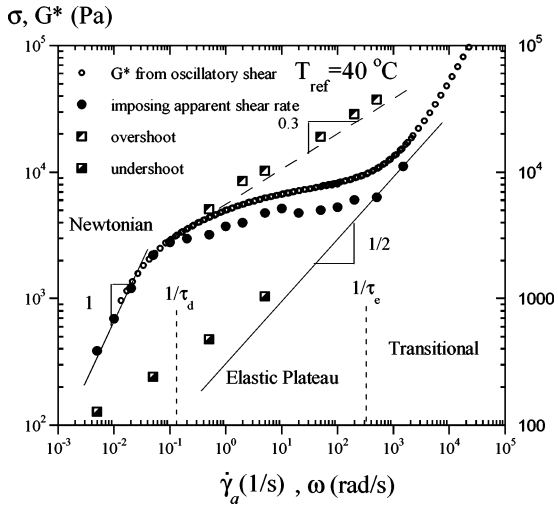

Figure 3. Oscillatory shear (open circles) and imposed-constant-velocity (filled circles) measurements at a reference temperature 40 °C of 10% PBD solution (based on oBD1). The filled circles represent the steady-state values of the resulting shear stress, and the half-filled squares correspond to the peaks and valleys in Figures 2 and 4b, respectively. The two times of τ_d and τ_e divide the flow behavior into three regimes: Newtonian, plateau, and transitional.

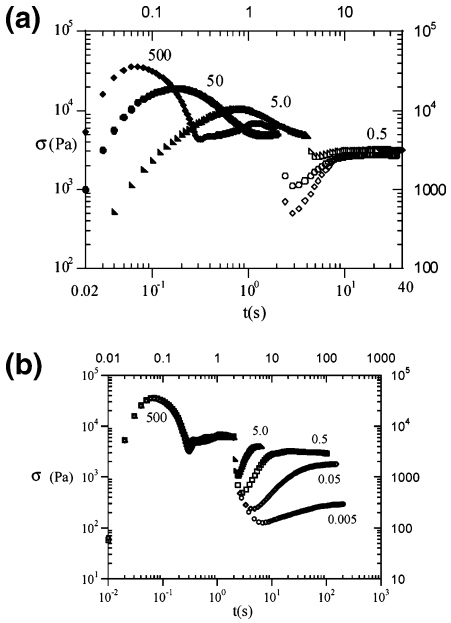

Figure 4. (a) Shear quench measurements in the mode of imposing constant velocity, stepping down from the plateau and transitional regimes to the end of the plateau regime, where distinctive stress undershoots are observed. (b) Shear quenches (in the mode of imposing constant velocity) from the beginning of the transitional regime into the plateau and Newtonian regimes.

of the plateau region. Specifically, the sample is respectively sheared at $\dot{\gamma}_a$ = 5, 50, and 500 s^{-1} and then quenched to $\dot{\gamma}_a$ = 0.5 s^{-1}. We observe distinct stress undershoot after the quench as shown in Figure 4a. In other words, a state of a lower viscosity created at the higher apparent shear rate survives for many seconds at the lower apparent shear rate of 0.5 s^{-1} before returning to the steady state corresponding to 0.5 s^{-1}.

In a separate set of experiments, we first sheared the sample just beyond the plateau region and then quench into various apparent rates in the plateau and terminal regions, as shown in Figure 4b. Undershoot follows the

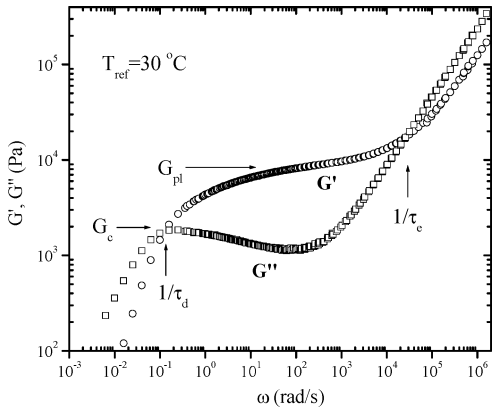

Figure 5. Master curves from oscillatory shear measurements using the time−temperature superposition at a reference temperature of 30 °C, where the crossover modulus G_c, plateau modulus G_{pl}, and the two relaxation times (which define the plateau width) are indicated.

shear quench in all cases. We have also plotted the minima of the undershoot in Figure 3 to give an indication that these points could be viewed as a downward extrapolation of an upper flow branch.

B. Controlled-Stress Experiments. Introductory Observations and Remarks. Before we carry out controlled-stress experiments, it is instructive to first investigate the linear viscoelastic behavior of the entangled polymer solution using oscillatory shear measurements and time−temperature superposition. Figure 5 shows the master curves of the storage and loss moduli G' and G'' vs frequency ω for the 10 wt % PBD/oBD2. The basic features of the master curves approximately agree with the scaling behavior described previously. For example, the plateau modulus G_{pl}, taken as G' at the frequency where G'' has a minimum, is around 8.0 kPa, which is close to the expectation from $G_{pl}(\phi) = \phi^{2.2}G_N^0$ for $G_N^0 = 1.2$ MPa. The plateau width depicted by the ratio τ_d/τ_e in Figure 5 is also close to the theoretical prediction. The physical significance of the rubbery plateau behavior for G' or G^* is well-known: A sample behaves like a rubber on a range of time scales shorter than τ_d because the entangled chains have no time to move away from one another. At lower oscillation frequencies than the reciprocal of τ_d, reptation-like diffusion can free the chains from their mutual entanglement in quiescence.

The most widely employed steady-shear experiment typically interrogates a sample in a cone−plate apparatus by rotating the lower plate with a certain angular velocity Ω. Then it is commonly assumed for the reasons discussed in section I that a simple shear with a uniform shear rate $\dot{\gamma}_a$ equal to Ω/θ would be produced in such a flow cell in absence of any secondary flow,[26] where the cone angle θ is very small and the subscript "a" is used explicitly here to indicate that Ω/θ is only the apparent or mean shear rate and could be different from the local shear rates across the gap in the stress plateau.

When $\dot{\gamma}_a\tau_d > 1$, a considerable amount of chain deformation and alignment takes place. The resulting stress would exceed the elastic plateau modulus $G_{pl}(\phi)$ as indicated by the stress maxima depicted by the upper-filled squares in Figure 3, had nothing happened to avoid the stress buildup. We are interested in identifying the correct mechanism that allows the sample to be sheared at increasingly higher apparent rates without much increase in the corresponding stress, i.e., the origin of the stress plateau behavior in Figure 3 observed using the mode of imposing constant velocity.

It is straightforward to view an entangled polymer on certain time scales as a soft solid with its strength comparable to its elastic plateau modulus $G_{pl}(\phi)$. The dynamic structure or transient network that makes the sample behave like a solid arises from chain entanglement. A natural question to ask would be whether imposing a shear stress comparable to $G_{pl}(\phi)$ would lead to "destruction of the network", e.g., to substantial disentanglement. More importantly, what is the condition for chain disentanglement? Would the level of disentanglement be a continuous function of the applied stress?

Yieldlike Behavior: Entanglement−Disentanglement Transition (EDT). The controlled-stress experiments to be depicted below attempt to answer these questions. It is clear from the discussion in section I that the conventional protocol of imposing constant velocity could by default only reveal a continuous relationship between the shear rate and shear stress. We examine the nonlinear flow behavior of the entangled PBD/oBD2 solution by applying different levels of shear stress using a stress-controlled Bohlin CVOR rheometer. At stresses well below $G_{pl}(\phi)$, the sample behaves in a simple way so that the generated shear rates soon approach steady values after the initial solidlike response. When the applied shear stress is higher than the crossover modulus G_c given by $G'(\omega_c) = G''(\omega_c)$ as indicated in Figure 5, a different kind of response is observed as shown in Figure 6a,b. In other words, below a critical stress level equal to G_c, the shear rate settles gradually to a steady-state value on a time scale of the order of the inverse shear rate. Above a shear stress level equal to G_c, the apparent shear rate is seen to rise in time by nearly 3 orders of magnitude. We indicate here "apparent" shear rate in Figure 6a,b because we currently do not have means to determine whether or not the local shear stress and shear rate would vary across the sample thickness during the transient period. The time required to reach the steady state depends so strongly on the level of the applied stress that we have presented the data separately in parts a and b of Figure 6 for the low- and high-stress conditions. The corresponding first-normal-stress difference N_1 changes with time in a much less distinctive manner, as shown in Figure 6c,d.

As far as we are aware, yieldlike flow transition observed in Figure 6a−d has never been reported for entangled polymer solutions or melts except in our recent communication.[27] Upon this transition, the sample exhibits a steady-shear viscosity as low as 20 Pa s at $\sigma = 3.0$ kPa in comparison to its value of 25 000 Pa s before the transition. Since the high zero-shear viscosity is universally regarded as due to chain entanglement, the reduction of 3 decades in the shear viscosity could be due to a massive loss of chain entanglement. Thus, we term this yieldlike constitutive transition an entanglement−disentanglement transition (EDT). At a microscopic level, chain disentanglement as the underlying molecular mechanism is just a conjecture. Although previous work has investigated the possibility of discontinuity in the flow curve,[12,13] no corresponding molecular mechanism has been suggested. Four potential alternative explanations are been examined in Appendices A−D and are found not to be responsible for the transition.

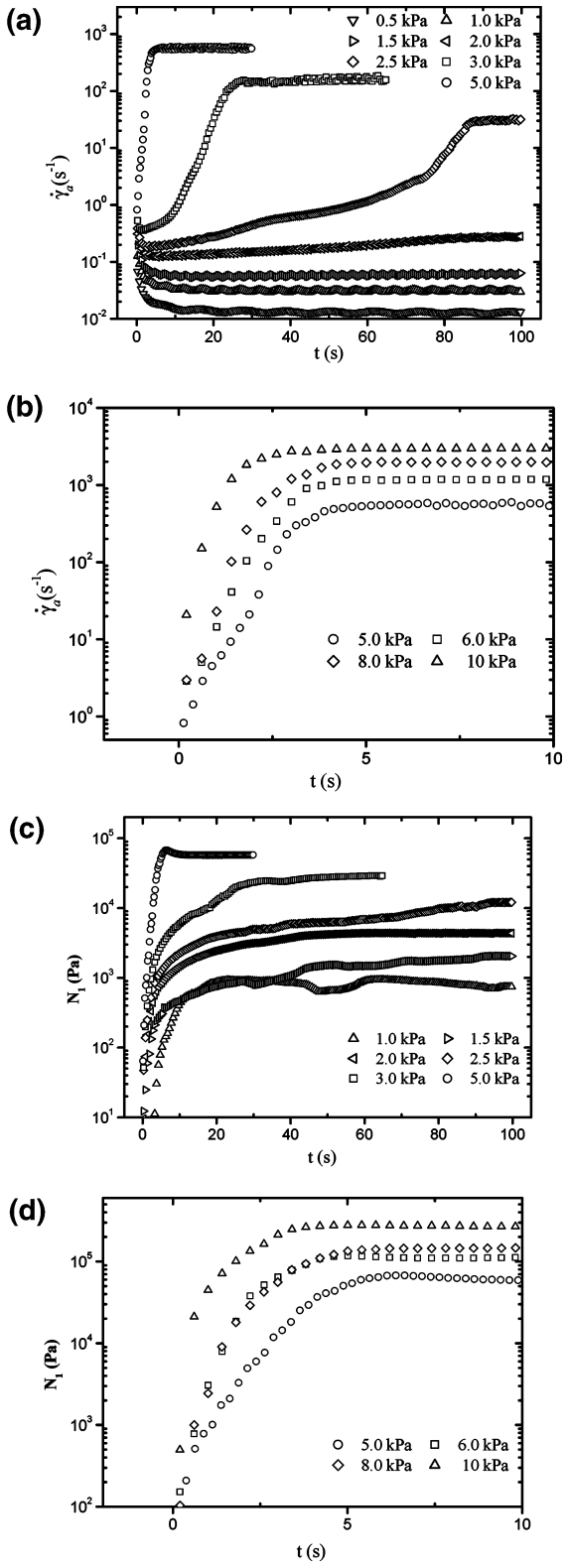

Figure 6. (a) Discrete creep experiments where a constant shear stress is applied and the resulting apparent shear rate $\dot{\gamma}_a$ is recorded as a function of time at 30 °C, where a different trend is seen for $\sigma \geq 2.5$ kPa. (b) Discrete controlled-stress experiments where the applied stresses ranges from 3.0 to 10 kPa. In contrast to (a), the rise of the apparent shear rate is much more rapid. (c, d) The corresponding normal stress N_1 measurements to those in (a) and (b), respectively.

The characteristic increase of the apparent shear rate with time as seen in Figure 6a,b occurs only when the applied stress is equally or higher than a critical value

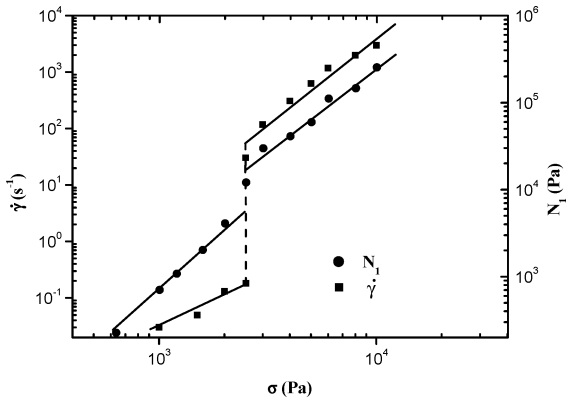

Figure 7. Steady-state values of the shear rate $\dot{\gamma}$ and normal stress N_1, read from Figure 6a–d, as a function of the applied shear stress σ, where the lower shear rate value at 2.5 kPa was taken from the initial value in Figure 6a.

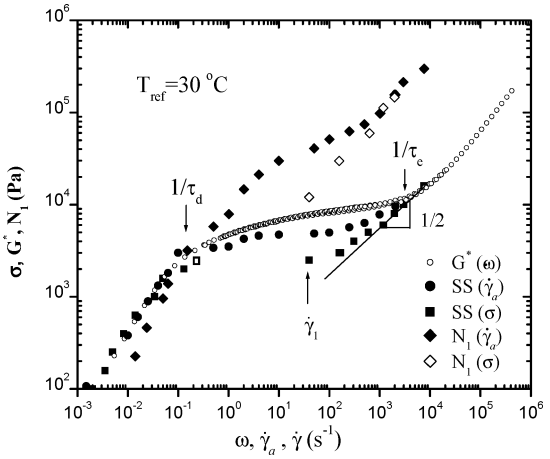

Figure 8. Steady-state flow curves of complex modulus $|G^*|$ vs frequency ω (open circles), shear stress σ vs apparent shear rate $\dot{\gamma}_a$ (filled circles) and vs true shear rate $\dot{\gamma}$ (squares) and normal stress N_1 vs apparent shear rate $\dot{\gamma}_a$ (filled diamonds) and vs true shear rate $\dot{\gamma}$ (open diamonds), obtained with oscillatory shear, imposing-constant-velocity ($\dot{\gamma}_a$) and imposing-shear-stress (σ) measurements, respectively. The imposing-constant-velocity measurements were carried out using ARES and also verified with Bohlin in its rate-controlled mode. The single open square, read from the minimum in Figure 6a at 2.5 kPa, underscores that for each value of the applied shear stress including σ_c there is only one value of shear rate in steady state.

of 2.5 kPa. For example, an applied stress of 2.4 kPa *does not* produce such a shear rate buildup. At 2.5 and 3.0 kPa, the apparent shear rate starts to increase when the normal stress N_1 approaches a level of 5.0 kPa, which apparently indicates a critical level of chain deformation required for the disentanglement transition. The steady-state normal stress N_1 above the transition is also noticeably higher than its value below the transition, as shown in Figure 7.

Comparing Imposing Shear Stress with Imposing Constant Velocity. It is important to contrast the respective flow responses of the entangled polymer solutions to imposed constant velocity and imposed constant shear stress. Figure 8 shows the steady-state flow curves obtained in these two respective modes. As a function of the apparent shear rate $\dot{\gamma}_a$, the resulting stress starts to saturate beyond a certain value of $\dot{\gamma}_a$. The flow behavior is very different under controlled stress: Beyond a critical shear stress the resulting shear rate jumps across the plateau region from the Newto-

nian branch to a Rouse-like branch. Upon a closer examination, it appears that the first accessible steady-state shear rate beyond the Newtonian branch is rather close to the frequency corresponding to the minimum of G'' in Figure 5. It remains for future studies to determine whether this is coincidental or generic.

The comparison between the filled squares and circles unravels something unexpected: The two steady-shear flow curves do not match. Specifically, in the controlled-stress experiment a wide range of shear rates is inaccessible in steady state beyond a critical stress level of ca. 2.5 kPa. Equally striking is the feature that the flow curves do not overlap even in the shear rate range accessible by both imposing-constant-velocity and imposing-shear-stress experiments; both the resulting shear and normal stresses are appreciably higher in the imposed-constant-velocity measurements. The loss of equivalence between these types of experiments clearly suggests that a uniform shear rate across the gap in the cone−plate flow cell may no longer be possible in the stress plateau region observed in the mode of imposing constant velocity. Anticipation of "shear banding" in the mode of imposing constant velocity has been anticipated previously in the modification of the original Doi−Edwards tube theory.[12,13] However, it remains to be seen whether the modified Doi−Edwards tube theory has the necessary ingredients to provide an adequate description of the experimental observations. In particular, the nonmonotonic constitutive curve envisioned with the modified Doi−Edwards model would anticipate the sample separating into two bands,[12,13] rather than a gradient in shear rate.

Finally we should note that although the disentanglement is substantial above the critical shear stress $\sigma =$ 2.5 kPa, it is perhaps still incomplete until $\sigma = 10.0$ kPa produced a shear rate equal to $1/\tau_e$, as indicated in Figure 8 (where the flow curves merge for different molecular weights and for the two different modes of shearing). We defer study of the effect of molecular weight on the constitutive transition to a future report.

IV. Additional Controlled-Stress Experiments To Explore the Nature of EDT

We carried out additional experiments designed to explore the necessary and sufficient conditions for producing chain disentanglement and to learn more about the characteristics of the nonlinear flow behavior observed in the controlled-stress mode.

A. Normal Stress Relaxation: Evidence for Coil−Uncoil Transition. The continuous rise of the normal stress N_1 during the transition as observed in Figures 6c,d is hardly distinguishable from that occurring below the transition. Nevertheless, the steady-state value of N_1 appears to display a small discontinuous jump as explicitly indicated in Figure 7. This leads to the question of how different the chain conformation becomes after the EDT. To explore the issue in some detail, we study the relaxation behavior of N_1 upon removal of the applied shear stress and compare the features obtained both below and above the EDT. Figure 9a shows that there was an initial rapid decay of $N_1(t)$ if the sample was first brought above the EDT, and there was no such signature if the sample was sheared below the EDT. It is striking that the first-step relaxation is complete within 5 s regardless of the shear stresses applied to produce the EDT. It is also worth noting that even after the first-step relaxation the residual N_1 can still be very high: For example, N_1 corresponding to $\sigma = 8.0$ kPa is higher in its second-step relaxation stage than that for $\sigma = 3.0$ kPa at the beginning of its relaxation.

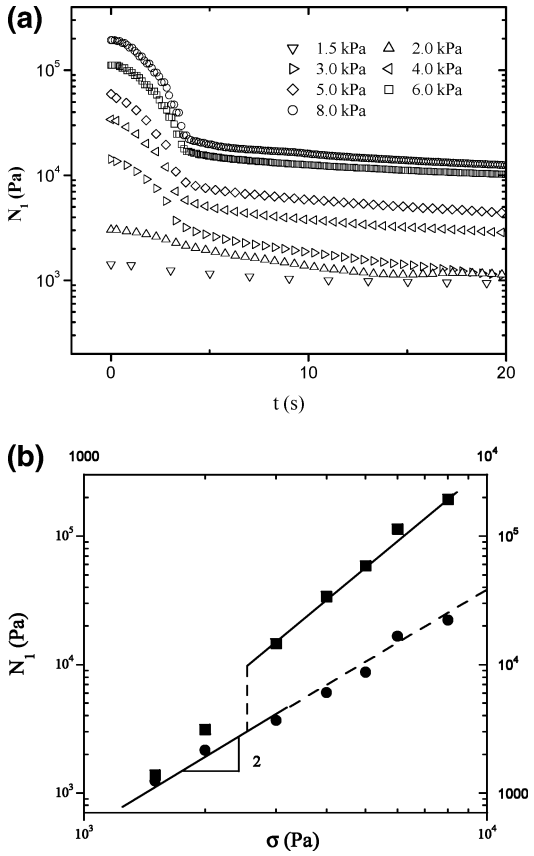

Figure 9. (a) Relaxation behavior of normal stress $N_1(t)$ at 30 °C upon withdrawal of the applied stress in the controlled-stress mode, where only two stresses are below the critical stress for the EDT, for which the characteristic two-step relaxation is absent. (b) Normal stress values below and above the EDT, obtained from (a) by taking $N_1(t = 0)$ as the squares and $N_1(t \sim 4$ s) as the circles, where the dashed vertical line indicates the location of the critical stress 2.5 kPa for the EDT for this 10% solution.

Since the normal stress is indicative of chain deformation, the two-step relaxation of $N_1(t)$ is particularly illuminating. We note that the two-step relaxation characteristic of N_1 is consistent with occurrence of a coil−uncoil transition (C−UCT)[28] after the EDT. The initial drop of N_1 reflects chain recoil from an uncoiled state only possible after the EDT. The magnitude of the first drop is actually similar to the discontinuity of N_1 observed in Figure 7 at the critical shear stress of 2.5 kPa. This characteristic of the normal stress relaxation dynamics can be explicitly expressed in Figure 9b, where the circles are taken from $N_1(t)$ at the end of the initial drop near $t = 4$ s and the squares are taken from $N_1(t)$ at $t = 0$ in Figure 9a. Figure 9b is reminiscent of Figure 7. The combination of Figure 7 and Figure 9a,b supports the suggestion that a C−UCT may have occurred following the EDT. The first rapid decay of N_1 as seen Figure 9a is not due to a rapid sample recoil upon turning off the shear stress because the same feature remains even if the sample continues to be sheared in the same direction as shown below in Figure 13b.

Upon further examining the dynamics of the EDT, it is clear that the chain disentanglement precedes the

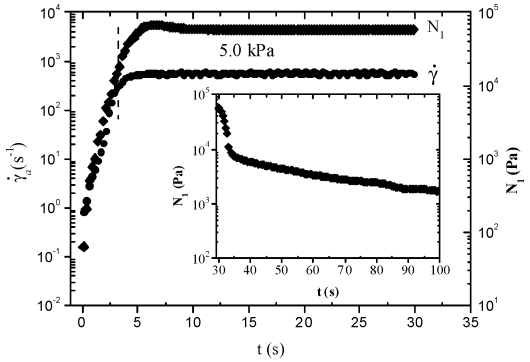

Figure 10. Comparison of the time-dependent buildup of the shear rate $\dot{\gamma}_a$ and normal stress N_1 at $\sigma = 5.0$ kPa to indicate the delayed approach of N_1 to its steady state. The inset shows the two-step relaxation of N_1 upon withdrawing the applied stress after the steady state at $t = 30$ s.

C−UCT. Figure 10 shows that further buildup of N_1 occurs after steady value is reached for the shear rate. Moreover, the growth of N_1 in Figure 10 after the EDT (denoted by the vertical dashed line) is of the same magnitude as the first drop in N_1 upon removal of 5.0 kPa at $t = 30$ s, as shown in the inset.

Finally, we note that the chain recoil as shown by the first-step relaxation of N_1 is much slower than can be depicted by the Rouse relaxation time, which can be estimated to be $\tau_R = [M_e(\phi)/M_w]\tau_d = 0.2$ s, knowing $\tau_d = 8.3$ s from Figure 5. The time scale involved in the first-tep relaxation of N_1 according to Figure 9a is actually comparable to τ_d.

B. Reshear after Preshear: Relationship between EDT and C−CUT. The normal stress N_1 continues to grow significantly after the vertical dashed line as shown in Figure 10. This increased normal stress may be attributable to a C−UCT mentioned above. One more crucial experiment is depicted here to show that the occurrence of the EDT does not actually require a C−UCT or existence of an excessively high normal stress (i.e., an excessive amount of chain deformation).

Since the transition described in Figures 6a,b, 7, and 8 is an entanglement-to-disentanglement transition (EDT), we would like to find out how long it takes for the system to recover chain entanglement and what level of chain alignment is required for the EDT. To explore these issues, we first bring the system into the transition by applying a sufficiently high shear stress and then allow the reentanglement to take place over time by turning off the stress. The data in Figure 11a,b are recorded in separate measurements with specified amounts of delay after the sample has been sheared at a given shear stress of 5.0 kPa into the steady state.

The combination of Figure 9a and Figure 11b indicates that the chain recoil restores chain entanglement effectively and that in absence of the recoil the disentanglement remains. In other words, after 5 s when the normal stress signal has completed its first-step relaxation, the sample has almost fully reentangled: The reapplication of 5.0 kPa produces an initial shear rate almost as low as its value for an equilibrium sample. On the other hand, for the 1 s delay the immediate shear rate is quite high as shown in Figure 11b, suggesting that reentanglement has hardly occurred during the interruption of 1 s. This appears to indicate that the chain recoil is necessary for the reentanglement.

A closer scrutiny of Figure 11a,b reveals several other important features. (I) Despite a high level of chain

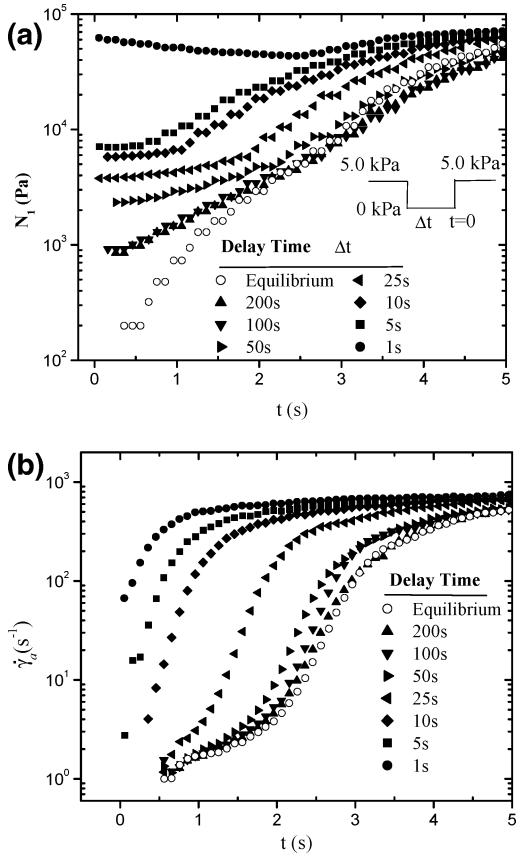

Figure 11. (a) Normal stress N_1 at 30 °C as a function of time after various delays before the reapplication of the shear stress of 5.0 kPa at $t = 0$, where at $t < 0$ the same stress of 5.0 kPa has been applied to produce the steady state as indicated by the drawing. (b) The corresponding apparent shear rate $\dot{\gamma}_a$ under the same conditions as described in (a).

orientation as indicated by the squares and diamonds in Figure 11a, the first square and diamond in Figure 11b indicates that there is little chain disentanglement. The disentanglement process simply takes a finite time t_{ss} to complete, and during t_{ss} the chain deformation as quantified by N_1 did not increase much correspondingly. (II) The left-pointing triangles indicate that the EDT completes just beyond $t = 2$ s when N_1 is still only as low as 6.0 kPa and has yet to grow another order of magnitude to its steady-state value. This is consistent with the observation made in Figure 10 and explicitly confirms that further rise in N_1 occurs after the disentanglement transition, a rise that we have suggested to originate from a coil−uncoil transition (CUCT). (III) A residual high level of chain orientation, as signified by the relatively high N_1 for delays up to 25 s, allows the EDT to be accelerated relative to the equilibrium sample.

C. Plausible Physical Pictures for Disentanglement and Reentanglement. The experiments shown in Figures 6a,b, 7, 8, 9a,b, 10, and 11a,b provide sufficient information to propose the following pictures pertaining to the chain disentanglement transition under shear and to the relaxation leading to the chain reentanglement upon withdrawal of shear.

(i) We first propose a description of the steps leading to the entanglement−disentanglement transition (EDT) in shear. Upon application of a sufficiently high shear stress, a critical level of normal stress (correlated with a critical amount of chain orientation S_c) takes place so

that the chain segments are no longer at "right angles" with one another, reducing their efficiency to mutually constrain. Here for lack of a more suitable symbol, we use S to denote the chain orientation or deformation in shear. We see from Figure 11a,b that $S > S_c$ is not a sufficient condition for chain disentanglement although it is a necessary condition. It appears that not only a sufficiently high shear stress σ ($\geq\sigma_c$) is required to maintain S_c, but more importantly the sample must suffer sufficient shear strain, allowing rearrangement of the topological relationship among all the chains in the sample so as to free chains from constraining one another. In other words, a finite time is required for the shear flow to reorganize the dynamic structure (entanglement) of the entangled solutions and to relieve chains from their mutual constraint, leading to the ultimate EDT. Once the chain entanglements are removed so are the bearers of the shear stress. Consequently, the individual chains become "naked" and fully exposed to the viscous forces, a situation similar to dilute solutions. Unlike dilute solutions, a high level of shear stress is present at the EDT, resulting in a rather efficient production of a coil−uncoil transition (C−UCT) in shear flow, upon which uncoiled chain conformations such as dumbbell-like shapes are a predominant state.[29] In our highly entangled solutions, the EDT appears to be a necessary and sufficient condition for C−UCT; i.e., a substantial C−UCT ensues after the EDT.

(ii) Upon removal of the shear stress after reaching the steady state, chain recoil takes place in such a manner as to reestablish the random topological relationship among the chains so that chain entanglement is restored. Since chain reentanglement is triggered by the chain recoil, the latter is often incomplete. In other words, the restored chain entanglement due to the recoil arrests (i.e., slows down) any further chain recoil that could potentially take place rapidly in absence of chain entanglement. This is rather evident from Figure 9a: the comparison between the right-pointed triangles and circles as well as squares indicates that there is still a great deal of residual N_1 for $\sigma = 6.0$ and 8.0 kPa after the first-step relaxation, which is higher than N_1 at steady state for $\sigma = 3.0$ kPa. In other words, the level of chain anisotropy is still higher for $\sigma = 6.0$ and 8.0 kPa after the first-step relaxation than that for $\sigma = 3.0$ kPa in steady state.

To summarize the emerging picture concerning the nonlinear flow behavior of entangled solutions, we present a cartoon in Figure 12 that depicts what we think happens during the entanglement−disentanglement transition (EDT) in shear and the reentanglement upon chain recoil and relaxation. The description is for a highly entangled monodisperse polymer system. Figure 12b,d depicts the different stages during the EDT at a constant shear stress. When we vary molecular weight and its distribution (MWD), there are modifications to this cartoon. For example, for shorter chains the C−UCT will be much less distinctive. In the presence of polydispersity, chains at the high end of MWD may be sufficiently oriented to meet the condition for disentanglement, and the rest of the shorter chains may conceivably remain entangled with one another. The combined result is a distribution of different states of chain entanglement and conformational anisotropy. If a significant fraction of the chains is unable to disentangle with one another, a macroscopic flow transition may not be observable.

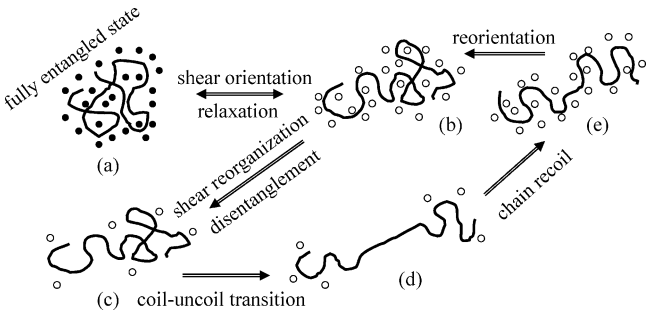

Figure 12. Steps leading to entanglement−disentanglement and coil−uncoil under constant-stress shear as well as chain recoil and relaxation from the disentangled state after turning off or sufficiently lowering the applied shear stress: (a) the equilibrium state where the chain is coiled and entangled as symbolized by the filled dots that represent full topological constraint of all chains on one another; (b) upon applying a sufficiently high shear stress all chains in the system reach a critical level of orientation so that it is now possible for the shear flow to alter the topological relationship among the chains, where the open dots explicitly indicate that the chains' constraining effect on one another is altered due to the significant chain anisotropy; (c) further shearing in time progressively reorganizes the system into a state where chains can avoid constraining one another so that there are hardly any constraining open dots, which is the state of disentanglement, where the corresponding shear viscosity may drop substantially; (d) the state of disentanglement in (c) allows individual chains to be fully exposed to viscous forces, which cause a conformation change from coil to uncoil; (e) upon turning off the shear stress, the chain recoil from state (d) efficiently restores chain entanglement. Note that although the state (e) is significantly more anisotropic than the disentangled state (c), it is already a state with full entanglement, as evidenced from Figures 11a,b and Figure 10. Finally, the relaxation of chain orientation from (e) to (b) is rather slow because of the existing chain entanglement. This is evident from Figure 9a and inset of Figure 10.

In passing, we should emphasize that chain disentanglement and subsequent uncoil require a substantial amount of continuous shear. According to Figure 6a,b, the EDT is complete only after hundreds of strain units took place and over another thousand strain units occurred before N_1 grew to its steady state presumably through a coil−uncoil process. This would explain why no significant chain alignment has been observed previously using SANS measurements.[30,31]

D. Absence of Hysteresis: EDT Is a Second-Order Transition. We carried out further experiments to explore the characteristics of chain disentanglement and reentanglement in shear flow. In particular, we would like to find out whether there is hysteresis associated with the constitutive transition.

For the 10% PBD solutions the crossover modulus G_c, where $G' = G''$, is around 2.0 kPa. Individual creep experiments indicate that the solutions remain on the lower Newtonian branch all the way up to 2.5 kPa. After 90 s, an application of shear stress equal to 2.5 kPa finally produced massive disentanglement, as seen in Figure 6a. Thus, the critical stress for disentanglement is close to 2.5 kPa, just above G_c. Figure 13a,b indicates that there is hardly any hysteresis in the sense that a shear stress of 2.4 kPa is unable to maintain a high shear rate even after the preshear at 5.0 kPa.[32] In other words, the EDT appears to be a second-order flow transition in contrast to the interfacial stick−slip transition, which is first-order.[33] The absence of hysteresis for EDT is due to lack of hysteresis for C−UCT in shear flow.

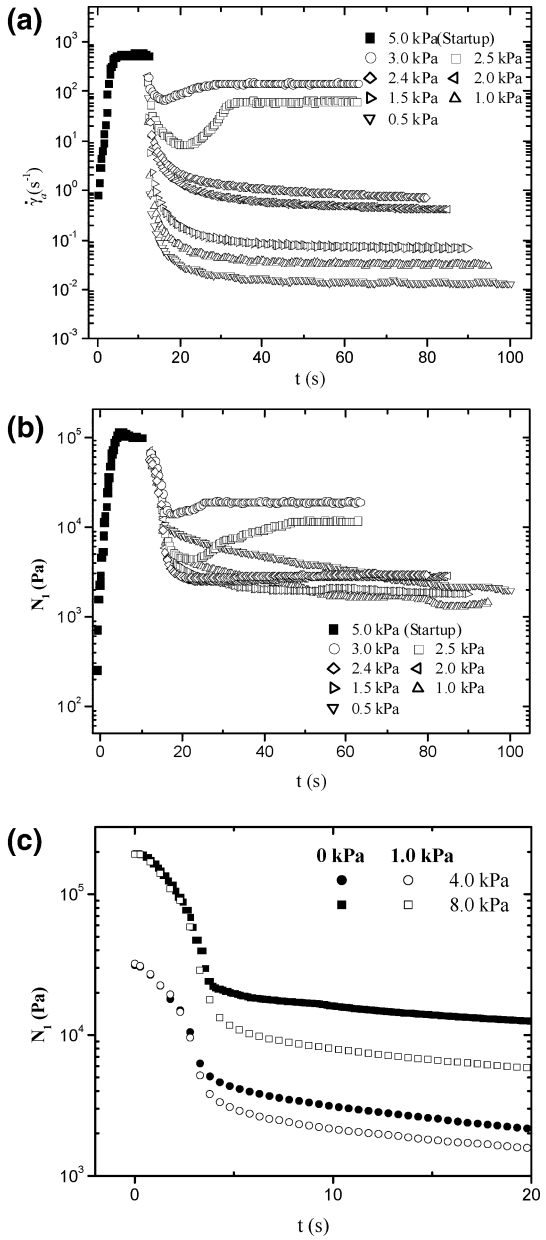

Figure 13. (a) Apparent shear rate $\dot{\gamma}_a$ at 30 °C as a function of time during the step-down experiments in controlled-stress mode from the initial stress of 5.0 kPa to the various stresses indicated. (b) The corresponding normal stress N_1 under the same conditions as in (a). (c) The normal stress relaxation after the attainment of the steady state at the two stresses of 4.0 and 8.0 kPa at $t = 0$ when either a stress of 1.0 kPa or zero stress replaces the higher stresses of 4.0 and 8.0 kPa.

In the case where the EDT is followed by a visible coil−uncoil transition (C−UCT) as is the case for the present solution, hysteresis would be possible if the C−UCT in shear flow would have hysteresis. However, the C−UCT is only expected to be second order in simple shear. The absence of hysteresis for C−UCT implies lack of hysteresis for the EDT because the chain recoil is shown in the combination of Figures 9a and 11a,b to efficiently restore chain entanglement. Our experiments confirm this expectation as we did not observe any measurable hysteresis for either EDT or C−UCT.

Finally, the normal stress data in Figure 13b indicate that the initial decay of N_1 at 0.5 kPa is of a smaller magnitude than that at the other higher shear stresses. This type of behavior is further confirmed by an additional experiment depicted in Figure 13c where in separate measurements the solution was first sheared with two stresses of 4.0 and 8.0 kPa into the respective steady states, and then the applied stress was either turned off or lowered to 1.0 kPa at $t = 0$. Similar to the behavior seen in Figure 13b, the initial decay of N_1 is smaller for the case where the flow is turned off. This observation confirms that the first-step rapid relaxation of N_1 is not originated from any sample recoil and indicates that the chain recoil process takes place more quickly due to the faster chain reentanglement aided by the weak shear.

V. Further Analysis and Comparison with Previous Work

Our controlled-stress experiments provide a phenomenological description of the constitutive relationship between the shear rate and shear stress. Specifically, we have roughly according to the squares in Figure 8

$$\sigma = \eta_0 \dot{\gamma} \qquad \text{for } \sigma < G_c \tag{1a}$$

and

$$\sigma/G_c = (\dot{\gamma}/\dot{\gamma}_1)^n \qquad \text{for } \sigma > G_c \tag{1b}$$

where we approximate the critical stress σ_c for the EDT by G_c defined in Figure 5 and $\dot{\gamma}_1$ is defined in Figure 8 as the first steady-state point of the transition in controlled-stress mode. Below the EDT, the sample viscosity η_0 is rather large, and the shear rates are relatively low. Upon the EDT, the shear rate jumps from about G_c/η_0 to $\dot{\gamma}_1$, or conversely the steady-shear viscosity drops from η_0 to $G_c/\dot{\gamma}_1$. The exponent n describes the flow behavior on the upper flow branch and is roughly around $^1/_2$, consistent with Rouse dynamics. There is clearly a discontinuity in the constitutive curve where a range of shear rates is inaccessible in steady state, implying existence of a shear rate gradient when such fluids are examined in a macroscopic flow cell using the mode of imposing constant velocity. Here multiple shear rates may exist across the sample thickness in steady state, and therefore the stress-optical rule seems to break down naturally because different states of chain conformation correspond to the same shear stress. It is also worth noting that eq 1a,b has little in common with the Bingham model.[34]

The $\alpha\beta$ component of the stress tensor σ for polymeric liquids is commonly given in the following generic form

$$\sigma_{\alpha\beta} \sim \int_0^L \mathrm{d}s\, [\langle u_\alpha(s,t)\, u_\beta(s,t)\rangle - \delta_{\alpha\beta}/3] \equiv \int_0^L \mathrm{d}s\, S_{\alpha\beta}(s,t) \tag{2}$$

where a proportionality constant is omitted, u_α and u_β are the projections of the vector of sth chain segment along directions α and β, respectively, L is the chain contour length, and $\langle\ \rangle$ represents the statistical ensemble average. To complete the description, one needs a dynamic equation depicting how the segment orientation occurs in flow. In other words, a theory must be developed to relate the segmental orientational tensor $S_{\alpha\beta}$ to a flow field such as simple shear with shear rate $\dot{\gamma}$. The Doi−Edwards tube theory[2] is one such attempt (but not the only one possible) to calculate $S_{\alpha\beta}$ for a given $\dot{\gamma}$ and to insert the result

$$S_{\alpha\beta}(s,t) = f(\dot{\gamma},t)|_{\text{tube}} \tag{3}$$

into eq 2 for a prediction of the constitutive relationship between σ and $\dot{\gamma}$. Equation 3 is symbolically the same, for example, as eq 7.194 in the Doi−Edwards monograph.[2] With increasing $\dot{\gamma}$, the tube becomes more aligned along the flow direction so that its projection in the velocity gradient direction continues to decrease, producing, for $\dot{\gamma} > \dot{\gamma}_d = 1/\tau_d$, a decreasing function of σ from eq 2, and creating the predicament of a stress maximum as sketched in Figure 1d, where τ_d is the terminal or reptation time. The reason for this unphysical prediction of the stress decline with increasing shear rate is that one still treats the system as entangled by preserving the tube picture and continues to apply eq 3 in eq 2 beyond $\dot{\gamma}_d$. What really happens for $\dot{\gamma} > \dot{\gamma}_d$ is actually rather different as discussed below.

Our current experimental findings suggest that at a shear rate $\dot{\gamma} > \dot{\gamma}_d$ the segmental orientation reaches a critical value of S_c, which is a necessary condition for chain disentanglement. Over time at $\dot{\gamma} > \dot{\gamma}_d$ full chain disentanglement would occur. In absence of chain entanglement, a new dynamic equation in place of eq 3 should be established to describe the chain orientation. Without the entanglement network the chain segments cannot be effectively oriented, and consequently the segmental orientation would drop below S_c, allowing chains to reentangle. The reentangled chains would suffer significant segmental orientation to reach the level of S_c, at which time chain disentanglement takes place again. Such an oscillation would perpetuate in time. This instability, during which the shear stress might fluctuate in time between the upper- and lower-filled squares in Figure 3, disappears only when $\dot{\gamma}$ is sufficiently high to keep the chains disentangled. If neither disentanglement nor reentanglement takes place collectively, the shear stress fluctuations may not show up in macroscopic measurements.

When a shear stress is the controlled parameter, the scenario is more straightforward. For $\sigma > G_c$, the chain segmental orientation exceeds the critical value of S_c, so that chains disentangle, with the prevailing shear rate reaching whatever value that would keep the chains disentangled. In this way we find a discontinuous steady-state constitutive relationship between shear stress and rate, as shown in Figure 1c, where the molecular origin of the discontinuity is chain disentanglement transition. In the window of the shear rate discontinuity no steady state can be established when shear rate is the controlled parameter. Upon the EDT, in the initial stage as depicted from Figure 12b to Figure 12c the chain segment orientation may not be much higher than S_c. A significant increase in the segmental orientation can occur from Figure 12c to Figure 12d as the chain undergoes the C−UCT, where u_x increases sharply but u_y drops substantially to keep the average of the product given in eq 2 unchanged. During the EDT from Figure 12b to Figure 12d, the dynamics governing $u_\alpha(s,t)$ can no longer be described by a tube theory because chain disentanglement is taking place.

In contrast to the preceding discussion, to describe the flow behavior for $\dot{\gamma} > \dot{\gamma}_d$ where the stress went over its maximum, it was previously envisioned[12,13] that eventually chain stretching occurred inside the tube at high enough shear rates to produce stresses as large as the stress maximum G_0 at $\dot{\gamma}_e \sim 1/\tau_e$, where τ_e is the tube confinement time. These studies resulted in converting the constitutive curve containing a maximum to Figure 1d and affirming a nonmonotonic feature of the constitutive relationship. However, there has previously been little discussion in the current literature of the physics governing the perceived flow discontinuity as indicated by the dashed line in Figure 1d.

In essence, a new molecular theory must be able to describe the disentanglement state and to replace eq 3 with

$$\mathbf{R}(s,t) = g(\dot{\gamma},t)|_{\text{disentanglement}-\text{reetanglement}} \tag{4}$$

where the vector $\mathbf{R}$, being the coordinate of the sth segment at time t, depicts the configuration of a test chain. The solution of eq 4 needs to be able to specify the range of shear rates (from $\dot{\gamma}_d$ to perhaps $\dot{\gamma}_e$), within which the segmental orientation may not find steady state and the chains may not have a fixed topological state. The theory leading to eq 4 would have to be able to predict the magnitude of the constitutive transition in terms of $\dot{\gamma}_1/\dot{\gamma}_c$, as shown in Figure 1c. Our present data shown in Figure 8 appear to indicate that $\dot{\gamma}_c \sim \dot{\gamma}_d$ and $\dot{\gamma}_1 \ll \dot{\gamma}_e$. Equation 4 must also describe the dynamics governing the temporal instability between the disentanglement and the reentanglement for a given local shear rate $\dot{\gamma}$ ($\dot{\gamma}_d < \dot{\gamma} < \dot{\gamma}_e$), where segmental orientation S would be an order parameter for chain disentanglement.

Equation 2 only accounts for the contribution from the intrachain forces. When the chains are extremely well aligned in shear after chain disentanglement and shear rate is rather high, interchain frictional forces may produce a significant contribution to the total shear stress. In other words, at sufficiently high stresses and shear rates perhaps above G_0 and $\dot{\gamma}_e$, respectively, we may have to add a new term to eq 2 to incorporate any internal friction effect. In summary, we consider all these factors as key ingredients of the next microscopic theory for entangled polymers, which quantitatively remains elusive at the present time.

It may be interesting to note, in passing, the extensive experimental[35,36] and theoretical activities[37,38] on the flow behavior of micellar solutions over the past 15 years took place mainly because such solutions also exhibit a stress plateau.[35,36] Unlike polymer solutions and melts, micelles are capable of adjusting their length in response to flow and also perhaps more prone to shear-induced segregation and phase separation. Some initial experiments[39] suggest that the rheological responses of entangled micellar solutions appear to be different depending on whether the mode of imposing constant velocity or the mode of imposing constant shear stress is employed. However, in our opinion, the nature of stress plateau observed for concentrations far below the borderline of the isotropic−nematic transition remains to be clarified. In particular, it may not share with entangled polymer solutions the same physics, especially in steady shear.

VI. Conclusion

In summary, through separate imposing-constant-velocity and imposing-shear-stress experiments we have investigated the nature of nonlinear flow behavior using model entangled polymer solutions. In particular, we have carried out controlled-stress experiments to examine the origin of the stress plateau seen in imposing-constant-velocity experiments. The observed yieldlike constitutive transition in controlled-stress experiments indicates clearly that the structure of the entangled

solutions, as depicted by the states of chain entanglement and of chain conformation anisotropy, is a discontinuous function of the applied shear stress σ. For example, the sample viscosity $\eta(\sigma)$ makes a sharp drop of 3 decades beyond a critical shear stress $\sigma_c = 2.5$ kPa for the present 10 wt % 1,4-PBD solution. We have suggested the molecular origin of this transition to be an entanglement−disentanglement transition (EDT). This idea of EDT will be subjected to extensive scrutiny in the future. Hopefully new experimental measurements beyond traditional rheological methods will be inspired to explicitly measure the state of chain entanglement in flow. It is our current opinion that the extensive data in the present paper are a great challenge for existing constitutive models[12,13,18] to reconcile with. Finally, we should add that if the conjecture of chain disentanglement as the origin of the observed flow transition is correct, similar nonlinear flow behavior is expected for monodisperse polymer melts. Polydispersity would simply contribute another layer of complexity to the already rather rich flow behavior.

Acknowledgment. This work is supported, in part, by the National Science Foundation through the Fluid Dynamics Program Grant CST-0115867. S.Q.W. thanks Alan Gent, Morton Denn, and Peter Olmsted for comments on the manuscript.

Appendix A. Contrasting with Interfacial Stick−Slip Transition

There are at least four factors that may differentiate an interfacial slip transition from the observed bulk flow transition, related to (I) the observed normal stress, (II) the surface condition, (III) the dependence of the shear rate on the sample thickness, and (IV) the magnitude of the transition.

(I) The stick−slip transition (SST) does not produce an increase in the bulk chain deformation so that the first normal stress difference is unchanged across the SST, in contrast to the normal stress jump at the transition, as shown in Figure 7, and the continuing increase of N_1 after the steady state of the measured shear rate is achieved, as shown in Figure 10.

(II) The SST can be removed by using organically coated surfaces to cause continuous wall slip through stress-induced polymer desorption. We have used Teflon-like surfaces for the cone−plate surfaces and see the negligible surface effect on the observed phenomena depicted in Figure 6a,b.

(III) As described below, the magnitude of a SST would show an explicit dependence on the dimension of the flow apparatus such as the sample thickness H. The yieldlike transition occurs not only in cone−plate but also in parallel plates. Using parallel plates, the magnitude of the transition is found to be independent of H as shown in Figure 14, where the vertical bar indicates the expected separation of the data if SST was responsible for the observed increase of the shear rate during the transition.

(IV) Finally, we can estimate the magnitude of a SST to compare with that of the observed flow transition. With the parallel-plate cell set at gap H, it is straightforward to estimate the jump in the apparent shear rate $\dot{\gamma}_{slip}$ due to interfacial slip

$$\dot{\gamma}_{slip}/\dot{\gamma}_{no-slip} = 1 + 2b/H \tag{A.1}$$

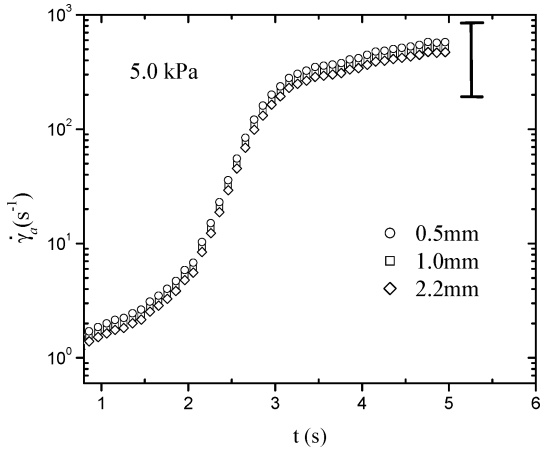

Figure 14. Apparent shear rate $\dot{\gamma}_a$ buildup at 5.0 kPa for different gap distances in a parallel-plate cell of 25 mm diameter.

relative to the actual rate $\dot{\gamma}_{no-slip}$ corresponding to no-slip boundary condition, in terms of the Navier−de Gennes extrapolation length[33]

$$b = (\eta/\eta_i)a_L \tag{A.2}$$

with a_L being the interfacial thickness where the chain disentanglement occurs. To estimate the upper bound for b, we take the interfacial viscosity η_i to be as low as that of the solvent η_s, which was measured to be 0.5 Pa s for oBD2. The shear viscosity η of the sample can be read from Figure 8 to be around 22 800 Pa s at 3.0 kPa. Inserting these values into eq A.2, we obtain $b < 45600a_L$, taking a_L to be the dilated tube diameter equal to $a\phi^{-0.6} = 17.5$ nm for $a = 4.4$ nm.[40] Thus, we have $b < 0.8$ mm. With a gap of 1 mm, we obtain $\dot{\gamma}_{slip}/\dot{\gamma}_{no-slip} < 2.6$. In contrast, the observed jump in the shear rate, measured in terms of the ratio of the steady-state shear rate to the initial transient value at 3.0 kPa, is around 460 according to Figure 6a instead of 2.6. Thus, the observed transition is clearly not an interfacial transition. We will consequently call it a constitutive transition to indicate that the transitional behavior is a bulk flow phenomenon.

Appendix B. Effect of Polymer Migration and Phase Separation in Shear

It has been suggested since the early 1990s by Doi and Onuki[41] that "composition inhomogeneity is created in mixtures of long and short polymers undergoing nonuniform flow". In particular, for a simple shear generated in a cone−plate rheometer, the long polymer would migrate toward the center of the flow cell according to Doi−Onuki. We would like to assess whether the flow behavior reported in this work would be related to the predicted development of radial polymer migration.

(I) The 3 orders of magnitude increase in the shear rate upon the EDT would require all long PBD chains to concentrate into a rather small radius at the center of the cone−plate cell, about 1/10th of the cone−plate radius to be precise, where the corresponding volume is much smaller than 10% of the total volume between the cone and plate. Since the solution contains 10 wt % of the long chains, this is physically impossible. Moreover, the normal stress would drop substantially in contradiction to Figures 6c,d, 10, and 11a, all of which indicate that the normal stress increases during the shear rate buildup.

(II) It would take a much longer time for any radial polymer migration to produce a rise in the measured shear rate than the time scales observed in Figure 6a,b, which can be as short as a few seconds.

(III) If the polymer migration would indeed happen, we should be able to estimate the time required for chain diffusion to homogenize the sheared sample after withdrawing the shear stress. Taking the largest diffusion coefficient to be dilute-solution-like, $D \sim k_B T/\eta_s R$ where η_s is taken to be as low as that of oBD2, which is 5 P, and R is the coil size around 100 nm for this PBD,[40] the time t for the chain diffusion to cover a distance of the cone radius $R_c \sim 10$ mm can be estimated as $t \sim R_c^2/D \sim 1.2 \times 10^9$ s at room temperature. But our experiment described in Figure 11b indicates that the sample returns to exhibit a shear rate nearly as low as an equilibrium sample does only 5 s after turning off the shear flow.

Finally, shear-enhanced concentration fluctuations have been observed in entangled solutions involving good solvents.[42] We are unable to perform conclusive light scattering measurements on the present solutions during shear because the refractive index difference between the 1,4-PBD and the solvent of oBD is rather small. We plan to explore this issue further in the future by using a small molecule solvent to ensure sufficient optical contrast. There may indeed be greatly enhanced concentration fluctuations upon the transition. However, we do not expect any concentration fluctuations to be the origin and therefore the cause of the transition. More importantly, we do not expect any shear-induced concentration fluctuations to produce different rheological responses to the two different modes of shearing. It will be helpful to carry out time-resolved rheooptical studies in the future to evaluate the level of concentration fluctuations upon the EDT relative to that below the EDT.

Appendix C. Estimating Viscous Heating

Viscous heating is commonplace during polymer flow. The key question is: given the temperature rise due to the viscous heating, how much would the sample viscosity drop due to the increased temperature? Our calculations indicate that under the worst-case scenario, i.e., at the highest stress applied, the largest possible temperature increase is around 19 °C. According to the temperature dependence for 1,4-PBD described by the WLF shift factor,[43] such a temperature increase from 30 to 49 °C can only cause the sample viscosity to drop by a factor of 2 and therefore cannot explain the viscosity drop of 3 orders of magnitude as observed in our experiments.

We have actually directly verified our analysis with IR measurements using an Omega HHM290 infrared temperature pyrometer. A 5 °C rise can be observed at 6 kPa in a cone−plate of 25 mm diameter after shearing for 10 s, which is fully consistent with our estimate. Finally we should note that the observed steady state in Figure 6a,b indicates the attainment of thermal equilibration between heat generation by viscous dissipation and heat transfer to the heat sink.

Appendix D. Issue with Sample Edge Fracture

Meniscus distortions frequently occur in drag flow such as cone−plate and parallel plate cells, and the subject has been previously reviewed.[23] A small scale irregular perturbation on the meniscus is thought to be controlled by the magnitude of the normal stress N_1. Edge fracture refers to the sample rolling around and out during shear. This leads to loss of contact between the sample and the shearing surfaces. This type of severe meniscus distortion is believed[23] to arise from a negative second normal stress difference N_2.

Edge fracture is found to be unimportant in our controlled-stress experiments and can be and is minimized in imposing-constant-velocity experiments by turning off shear right after the steady state has been reached. Little edge fracture is seen upon the EDT because the sample is now largely free of chain entanglement and possesses rather fast relaxation times to allow the free surface to comply with the moving boundary, i.e., the rotating cone. When sheared below the transition, our samples do not suffer from edge fracture because of insignificant accumulation of total shear strain. At the critical stress for the EDT, where the apparent shear rate builds up very slowly as shown in Figure 6a, some edge fracture has a chance to develop. Its negligible rheological effect can be verified by carrying out step-down experiment as shown in Figure 13a. In examining this point, we notice that the measured shear rates are identical from both step-up and step-down experiments as shown in Figures 6a and 13a for 3.0 kPa, but there is a small difference at the critical stress 2.5 kPa. This difference is interesting because it appears to be real. Any edge fracture during a step-up experiment at 2.5 kPa would only lead to a higher shear rate. However, the opposite is seen; i.e., the step-down experiment that was free of edge fracture actually produced a slightly higher shear rate.

References and Notes

(1) Ferry, J. D. *Viscoelastic Properties of Polymers,* 3rd ed.; Wiley: New York, 1980.
(2) Doi, M.; Edwards, S. F. *The Theory of Polymer Dynamics,* 2nd ed.; Clarendon Press: Oxford, 1988.
(3) Graessley *Adv. Polym. Sci.* **1974**, *16*, 1.
(4) Stratton, R. A. *J. Colloid Interface Sci.* **1966**, *22*, 517.
(5) Wagner, M. H.; Meissner, J. *Macromol. Chem.* **1980**, *181*, 1533.
(6) Lee, C. L.; Polmanteer, K. E.; King, E. G. *J. Polym. Sci., Part A-2* **1970**, *8*, 1909.
(7) Huppler, J. D.; et al. *Trans. Soc. Rheol.* **1967**, *11*, 181.
(8) Crawley, R. L.; Graessley, W. W. *Trans. Soc. Rheol.* **1977**, *21*, 19.
(9) Menezes, E. V.; Graessley, W. W. *J. Polym. Sci., Polym. Phys. Ed.* **1982**, *20*, 1817.
(10) Bercea, M.; Peiti, C.; Simionescu, B.; Navard, P. *Macromolecules* **1993**, *26*, 7095. The 2% solution in this paper appears to be off by a factor of 10 in terms of its viscosity in comparison with that of the 6% solution. Since the plateau stress values are reasonable for both solutions, it seems that the molecular weight in the 2% solution is only half of that in the 6% solution.
(11) Pattamaprom, C.; Larson, R. G. *Macromolecules* **2001**, *34*, 5229.
(12) McLeish, T. C. B.; Ball, R. C. *J. Polym. Sci., Polym. Phys.* **1986**, *24*, 1735. Although this work was motivated to offer an explanation for the spurt effect that was later proved to be interfacial in origin, it carried a flavor of accounting for "a discontinuity in the flow curve of monodisperse melt in capillary".
(13) Cates, M. E.; McLeish, T. C. B.; Marrucci, G. *Europhys. Lett.* **1993**, *21*, 451.
(14) Marrucci, G. *J. Non Newt. Fluid Mech.* **1996**, *62*, 279.
(15) Mead, D. W.; Larson, R. G.; Doi, M. *Macromolecules* **1998**, *31*, 7895.
(16) Milner, S. T.; McLeish, T. C. B.; Likhtman, A. E. *J. Rheol.* **2001**, *45*, 539.
(17) Marrucci, G.; Ianniruberto, G. *Philos. Trans. R. Soc. London A* **2003**, *361*, 677.
(18) Graham, R. S.; Likhtman, A. E.; McLeish, T. C. B.; Milner, S. T. *J. Rheol.* **2003**, *47*, 1171 and references therein.

(19) Read, D. J. *J. Rheol.* **2004**, *48*, 349.
(20) de Gennes, P. G. *Scaling Concepts in Polymer Physics*; Cornell University Press: Ithaca, NY, 1979. de Gennes, P. G. *J. Chem. Phys.* **1971**, *55*, 572.
(21) Subsequently we choose to use the term "mode of imposing constant velocity" instead of "controlled-rate mode" to avoid any confusion about the true meaning of this conventional protocol.
(22) Yieldlike flow transition is rather commonly observed for systems such as concentrated suspensions, foams, gels, and even granular materials. See: Evans, I. D. *J. Rheol.* **1992**, *36*, 1313.
(23) Larson, R. G. *Rheol. Acta* **1992**, *31*, 213.
(24) Struglinksi, M. J.; Graessley, W. W. *Macromolecules* **1985**, *18*, 2630.
(25) Yang, X.; Wang, S.; Ishida, H. *Macromolecules* **1999**, *32*, 2645.
(26) Hoppmann, W. H.; Miller, C. E. *Trans. Soc. Rheol.* **1963**, *7*, 181. Secondary flow is observed in this study for even a Netwonian fluid because of the unusually large cone angles employed.
(27) Tapadia, P.; Wang, S. Q. *Phys. Rev. Lett.* **2003**, *91*, 198301. A phenomenologically similar observation is known as spurt or stick−slip transition (SST)[33] in capillary flow of highly entangled polymers, where the shear stress varies linearly with the radius and is highest at the wall. In that case the first transition to observe upon gradually increasing the applied pressure must involve the very first layer of the material. In other words, such a transition would be sharp and interfacial in nature. Because of the stress gradient, no abrupt transition would be observable at higher pressures in contrast to the present case of cone−plate geometry where the shear stress is presumably uniform and every layer undergo "chain disentanglement", leading to the bulk flow transition.
(28) A related concept is coil−stretch transition. There are only two cases where the concept of coil−stretch transition (C−ST) is invoked. The first, also most extensively studied, involves subjecting a dilute polymer solution to flow, as exclusively analyzed by de Gennes (*J. Chem. Phys.* **1974**, *60*, 5030) and recently verified (Schroeder, C. M.; et al. *Science* **2003**, *301*, 1515). In the second case, the C−ST occurs to the tethered (or adsorbed) chains during a stick−slip transition. We use the word "uncoil" instead of "stretch" because the word "stretch", as used repeatedly in most of the recent theoretical publications such as refs 16 and 18, implies that the contour length exceeds its equilibrium value, and the increase of the contour length is continuous with respect to the flow condition. See footnote 29 for a more precise depiction of the uncoil state in our picture.
(29) We specifically avoid using the well-established concept of coil−stretch transition (CST) because CST is commonly used to refer to flow-induced conformational change in dilute solutions. Regarding C−UCT, we would make the following speculations: The C−UCT does not have to involve the entire chain. Portions of the chain may remain coiled. The uncoiled part is predominantly the middle portion of the chain, where conformations are stretched and oriented in shear. In other words, we expect the dumbbell-shaped chain conformation to be statistically dominant. Multiple-dumbbell, half-dumbbell, and hairpin conformations may also be present. As higher shear stresses are applied, i.e., marching up along the upper flow branch, two things will happen: (a) the fraction of the chain still in the coil conformation diminishes; (b) the uncoil portion can and will become "thinner" beyond $1/\tau_e$, i.e., the uncoiling will involve straightening the chain backbone. Eventually at higher stresses yet, the uncoiling may look more like stretching, and coil−uncoil develops into coil−stretch.
(30) Muller, R.; Pesce, J. J.; Picot, C. *Macromolecules* **1993**, *26*, 4356. In this work, a polystyrene sample between parallel plates was sheared in linear displacement at a sufficiently high stress of 0.2 MPa for a total strain of up to 4, far less than what is perhaps necessary to produce a state of high chain orientation.
(31) Bent, J.; et al. *Science* **2003**, *301*, 1691. In this work, polystyrene is subjected to a channel flow, where the maximum level of shear strain is approximately $6L/H = 48$, and the averaged strain is only 24, which may not be sufficient to produce chain disentanglement and uncoiling. In channel flow, only a small fraction of sample near the wall is under high shear. It is not surprising that only a small amount of averaged chain anisotropy is observed in such a flow apparatus under the specified flow condition.
(32) The "hysteresis" points reported in Figure 1 of ref 27 were taken from a similar "hysteresis" experiment. In other words, those half-filled circles were similar to the data corresponding to 2.5 and 3.0 kPa. Since the 10% solution based on oBD1 is much slower, we did not shear the sample long enough at those stresses for it to make the EDT. Given longer durations of shear, we would have found those half-filled circles to be the filled circles in ref 27. In other words, there is no true hysteresis.
(33) Wang, S. Q. *Adv. Polym. Sci.* **1999**, *138*, 227. The interfacial stick−slip transition exhibits hysteresis and is first order because the coil−stretch transition responsible for the wall slip involves the tethered (naturally adsorbed) chains. For these tethered chains, the shear flow is equivalent to an elongational flow.
(34) Bingham, E. C. *Fluidity and Plasticity*; McGraw-Hill: New York, 1922; pp 215−218. The Bingham expression can be found in popular monographs such as: Bird, R. B.; Armstrong, R. C.; Hassager, O. *Dynamics of Polymeric Liquids*; Wiley & Sons: New York, 1987; p 228. Macosko, C. W. *Rheology*; VCH: New York, 1994; p 92. Unfortunately, the Bingham formula does not describe a yieldlike transition correctly because upon yield the shear rate attains a finite value instead of increasing continuously from zero as described by Bingham.
(35) Rehage, H.; Hoffmann, H. *Mol. Phys.* **1991**, *74*, 933.
(36) Lerouge, S.; Decruppe, J. P.; Berret, J. F. *Langmuir* **2000**, *16*, 6464.
(37) Spenley, N. A.; Cates, M. E.; McLeish, T. C. B. *Phys. Rev. Lett.* **1993**, *71*, 939.
(38) Radulescu, O.; et al. *Europhys. Lett.* **2003**, *62*, 230.
(39) Grand, C.; Arrault, J.; Cates, M. E. *J. Phys. II* **1997**, *7*, 1071.
(40) Fetters, L. J.; Lohse, D. J.; Richter, D.; Witten, T. A.; Zirkel, A. *Macromolecules* **1994**, *27*, 4639.
(41) Doi, M.; Onuki, A. *J. Phys. II* **1992**, *2*, 1631.
(42) Endoh, M. K.; Saito, S.; Hashimoto, T. *Macromolecules* **2002**, *35*, 7692.
(43) See Figure 5c in: Wang, S.; Wang, S. Q.; Halasa, A.; Hsu, W.-L. *Macromolecules* **2003**, *36*, 5355 for the temperature dependence of the 1,4-PBD viscosity, which shows that the viscosity of 1,4-PBD drops to half of its value as the temperature changes from 30 to 49 °C.

MA0490855